scientific reports

OPEN

Implantable small ultra-wideband circularly polarized antenna design for continuous blood pressure monitoring

Zhiwei Song✉, Xianren Zheng, Youwei Shi & Yuchao Wang

This paper presents a miniaturized circularly polarized (CP) implantable antenna Ultra-wide bandwidth for continuous blood pressure monitoring. The miniature and CP of the antenna are gained by using a new slot method. The symmetry slots in the radiation patch, two T-shape slots in the GND, coupled with the use of a short pin make the designed antenna with good physical and radiation properties. In simulation, the fractional effective axial ratio bandwidth is 23.6% (2.36–2.94 GHz), and the peak gain is − 28.9 dBi. Its total size is only 17.78 mm³ ($0.056 \times 0.04 \times 0.004\ \lambda_0^3$), which size is smaller compared to other antennas with similar performance. A prototype is fabricated and measured. The experimental results are in good agreement with the simulation results. And, the radiation patterns have good symmetry both in the simulation and measurement. In addition, the maximum SAR value is in accordance with the IEEE standard safety guidelines (IEEE C95.1-2019).

With the increasing demand for wireless medical solutions with implantable medical concerns, implantable antennas for wireless biomedical applications have become one of the most talked about technologies. In order to have a detailed understanding of a patient's health condition, health condition monitoring is needed in daily life[1]. Examples include blood pressure and glucose monitoring[2–4], capsule endoscopy[5,6], and leadless pacemakers[7–9]. For blood pressure monitoring, a blood pressure monitoring device can be implanted near the artery in the human arm. The sensor measures the pressure changes in the artery and converts them into electrical signals, which are then amplified, filtered, and converted into digital signals for processing and transmission. The implantable antenna transmits the blood pressure data to an external device for storage and processing, ultimately providing accurate blood pressure data to help doctors monitor the patient's blood pressure.

Implantable antennas must be implanted into the patient's body. To ensure the patient's comfort, the miniaturization of the antenna is crucial. Common miniaturization methods include: using substrates with a high dielectric constant[10]; introducing active elements[11]; designing the radiation patch into a serpentine structure[12,13]; opening U-shaped variant slots[14–16]; opening variant slots based on the inverted F structure and adding short-circuit vias to introduce the electrical load effect[16]. [17] by using a spiral radiator with two symmetrical arms and introducing an open-ended slot in the ground, the antenna's size is significantly reduced, and its volume is only 17.15 mm³ (7 mm × 6.5 mm × 0.377 mm). Working in the complex electromagnetic environment of the human body, while achieving miniaturization, it is also necessary to expand the bandwidth as much as possible and enhance the anti-interference ability. Using low-loss, flexible biocompatible materials such as polyamide[18] or Taconic CER-10[19,20], or embedding curved slots[21], zigzag slots[22,23] and C-shaped slots[24] in the radiation patch and ground of the antenna can significantly reduce the antenna size while obtaining good bandwidth performance. Among them,[25] proposed an ultra-miniaturized antenna with a volume of only 10.66 mm3 and an ultra-wide bandwidth of 3040 MHz (0.79—3.83 GHz) for leadless pacemakers. [26]introduced an antenna design for wireless capsule endoscopes, and the frequency bandwidth of this antenna ranges from 0.61 to 1.51 GHz, with a fractional bandwidth (FBW) of 84.91%. However, the above work is mainly based on linear polarization. Considering the continuous change of the position of the monitoring equipment in the human body linear polarization may not be sufficient. Therefore, circularly polarized (CP) antennas become an effective solution to this problem. The use of reactive impedance substrates (RIS) design[27], symmetric L-shaped slots on the radiation patch[28], curved slots[29] and slit rings[30], etc. among which[30], the designed implantable antenna achieves circular

School of Electrical Engineering, Xinjiang University, Ürümqi 830047, China. ✉email: suzawer@163.com
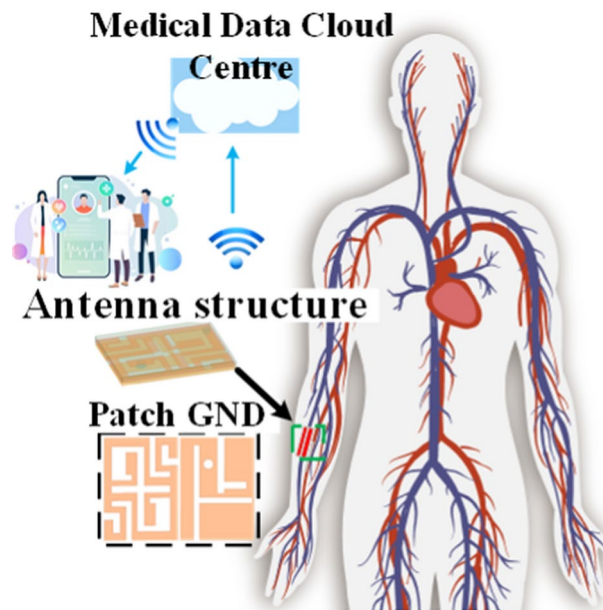
Fig. 1. Antenna implanted in the right-hand arm model.

polarization in three frequency bands. These designs have been cleverly applied to the miniaturization, circular polarization, and bandwidth expansion of patch antennas, providing ideas for our research.

This paper presents a novel miniaturized ultra-wideband CP implantable antenna that operates in the ISM band, has a very small size (17.78 mm^3) and a simple structure for continuous blood pressure monitoring. Miniaturization and matching of the desired frequency are achieved by introducing a through-hole between the rectangular radiator and the ground plane, etching two asymmetric T-slots on the ground plane, etching a cross-shaped slot in the middle of the radiating unit, and etching four L-slot curves on the edges. Meanwhile, the bandwidth adjustment and AR bandwidth expansion were achieved by adjusting two asymmetric T-slots in the ground plane. The depth of the implanted three-layer model (skin-fat-muscle model) was 11 mm at 2.45 GHz operating frequency, as shown in Fig. 2d. An impedance bandwidth of 46.5% (1.85–2.99 GHz), a maximum gain of −28.8 dBi, and an AR bandwidth of 23.6% (2.36–2.94 GHz) were achieved. In order to realistically simulate the usage environment, we also simulate it in the arm model, as shown in Fig. 1. The geometry of the antenna and parameters are shown in Fig. 2a–c, and the values are listed in Table 1. SAR and maximum input power calculations are also performed for this antenna system for safety reasons (Table 2). The designed antenna is compared with the same type of work as shown in Table 3. Compared to[28] and[29], our design has some advantages in terms of size, BW and ARBW. The antenna in[30] is a very good job, it has three working frequency bands with high gain, but its absolute size (50.8 mm^3) is large due to it covers low frequency band. Compared with[31] and[32], our work is slightly inferior in terms of the electrical length size at the lowest operating wavelength and gain, but has a very obvious advantage in terms of bandwidth and circular polarization. Finally, the designed antenna has been fabricated and experimentally verified in a crushed pork and the results show that the antenna has excellent impedance bandwidth and circular polarization bandwidth performance.

Topology and design strategy
Geometry of the antenna
The structure of the ultra-wideband CP antenna is shown in Fig. 2a–c. Rogers 6010 with dielectric constant εr = 10.2, tangent loss tan(δ) = 0.0027, and thickness of 0.254 mm was selected for both the antenna substrate/covering layer. The use of a material with high dielectric constant as the substrate reduces the resonance frequency and thus achieves the size reduction. In order to further miniaturize the antenna, a thin layer of the substrate covering and the short-circuiting probes are added, while the resonance frequency is shifted to a more lower frequency band to obtain a highly miniaturized antenna (antenna size of 0.056 × 0.04 × 0.004 λ03). The addition of the cover layer brings some additional advantages, as it not only protects from contact with human tissue, but also stabilizes fluctuations in the effective dielectric constant around the antenna. Since a symmetrical layout is prone to circular polarization, four L-shaped slots symmetrical about the origin and one cross-shaped slot are cut diagonally in the radiating patch. Two asymmetric T-shaped slots cut in the ground plane help to extend the impedance bandwidth and AR bandwidth. In addition, the 50 Ω coaxial feed that excites this antenna is located at (x, y), and the short-circuit probe is placed at the optimal position in the upper left corner (N4). Together these designs achieve good miniaturization, impedance bandwidth and CP characteristics.

Simulation setup and environment
The design and simulation experiments are carried out in the High Frequency Structure Simulator (HFSS) computed using the finite element method, and considering the interaction with biological tissues, the
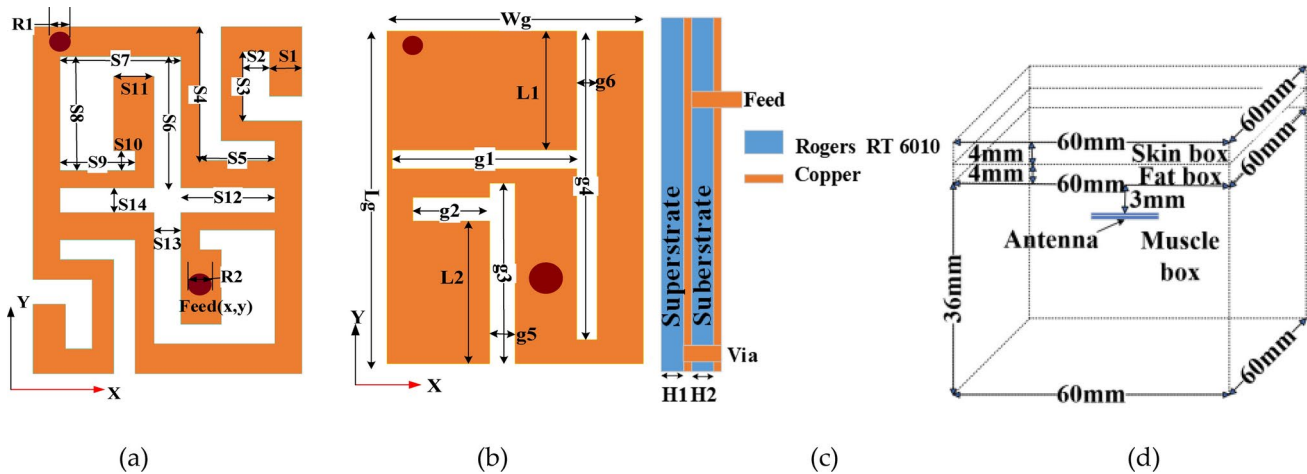
Fig. 2. Geometry of antenna. (**a**) Radiation plane. (**b**) Ground plane. (**c**) Side view. (**d**) Three-layer mode.

Parameters	Value	Parameters	Value	Parameters	Value
S1	0.6	S11	0.75	L1	2
S2	0.5	S12	1.7	L2	3
S3	1.4	S13	0.3	x	0.6
S4	2.7	S14	0.4	y	1.7
S5	1.4	Wg	5	H1	0.254
S6	2.7	Lg	7	H2	0.254
S7	2.2	g1	3.6	R1	0.4
S8	2.3	g2	1.5	R2	0.44
S9	1.4	g3	3.8		
S10	0.4	g4	6.5		

Table 1. Geometric parameters optimized for the proposed antenna (unit: mm).

2.45 GHz	Skin	Fat	Muscle
ε_r	38.0	5.28	52.729
Conductivity (S/m)	1.464	0.104	1.739
tan(δ)	0.283	0.145	0.242

Table 2. Relevant dielectric properties of tissue models at 2.45 GHz.

Ref.	Dimensions ($\lambda_0 \times \lambda_0 \times \lambda_0$)	Fre. (MHz)	SAR (1−g)	BW (MHz)	Gain (dBi)	CCP	AARBW
[26]	0.093×0.046×0.0001	915	202	900	−34	No	–
[28]	0.025×π2×0.0102	2450	856.4	400	−37.3	Yes	22%
[29]	0.028×0.028×0.0012	1400 2450	256.9 152.6	240 313	−32.7 −25.9	Yes	– 11.4%
[30]	0.028×0.028×0.003	860 1850 2450	428 438 382	135 139 458	−31.8 −21.8 −18.5	Yes	23.85% 1.37% 7.26%
[33]	0.03×0.03×0.007	920	552	800	−23.3	Yes	21.87%
[34]	0.041×0.041×0.002	1400 2450	178.2 122.1	180 640	−23.4 −16	Yes	9.7% 15%
This work	0.056×0.04×0.004	2450	652.3	1400	−28.8	Yes	23.6%

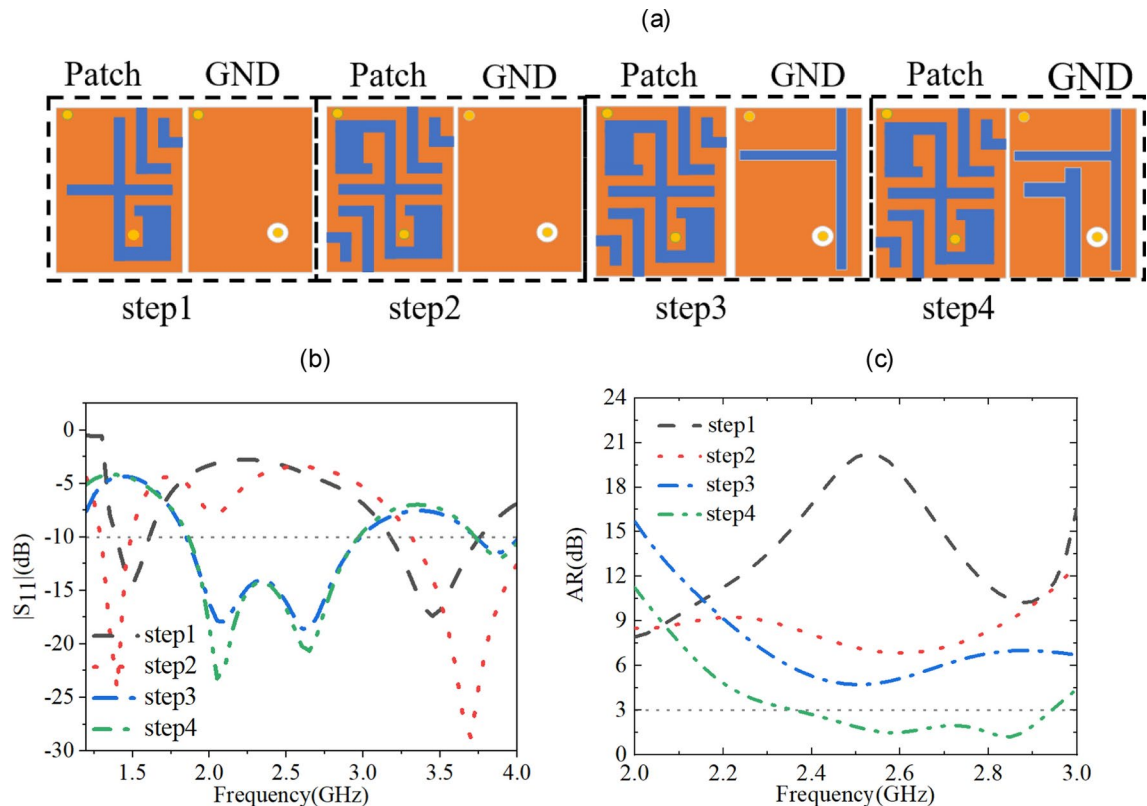**Table 3.** Proposed antenna comparison with references.

Fig. 3. (**a**) Design steps. (**b**) $|S_{11}|$ for each step of the design. (**c**) AR for each step of the design.

implantable antenna of our design is embedded in a three-layer model (skin-fat-muscle) with the dimensions of $(60 \times 60 \times 44)$ cubic millimeters for the simulation, and the relevant dielectric properties of the tissue model at 2.45 GHz are shown in Table 2[30,31], in which The thickness of both the skin and fat layers is 4 mm, the thickness of the muscle layer is 36 mm, and the tissue is surrounded by a $100 \times 100 \times 100$ mm³ cubic radiation box. The device was then simulated in a three-layer model. After meeting the desired requirements, the device was implanted in ground pork to a depth of 11 mm for actual measurements. This provided a reliable performance benchmark for practical in vivo implantation applications.

Antenna design

The designed antenna achieves the design requirements in four steps. First, the original dimensions of the antenna are calculated by the following formula[30]:

$$fr = \frac{c}{\lambda g \sqrt{\varepsilon eff}} \approx \frac{c}{Lg\sqrt{\frac{\varepsilon r+1}{2}}} \qquad (1)$$

where f_r is the resonant frequency, λ_g represents the guided wavelength, ε_{eff} represents the effective permittivity, ε_r is the relative permittivity, and Lg is the length of the antenna. The resonant frequency of the traditional patch antenna is 3.94 GHz. The design starts with a patch antenna with a complete ground plane and the introduction of a short-circuit probe. Firstly, in Step I, the patch antenna is slotted in an L-shape and cross shape to extend the current path and increase the capacitive effect, resulting in a reduction of the antenna resonance to 1.5 GHz. Meanwhile, the cross-shaped slot also excites resonance at 3.4 GHz, but this does not meet the requirements for working in the ISM band. Therefore, the patch is further slotted, and due to the symmetrical layout that tends to produce CP, the slots are symmetrically centered on the origin of the antenna. This causes the frequency to decrease to 1.4 GHz and 2.2 GHz, and a resonance is generated at 3.7 GHz, and the AR curve becomes flatter. However, as shown in Step II, the result is still unsatisfactory. For the existing resonance frequencies that need to be moved to a satisfactory band, some changes must be made to the ground plane. Therefore, in Step III, the circuit path is further expanded by slotting and the capacitive effect is increased by creating an asymmetric T-slot in the ground plane. The introduction of the asymmetric T-slot allows the antenna to combine the two adjacent modes in Step II, forming a wide bandwidth between 1.85 GHz and 2.99 GHz. At the same time, the AR curve becomes flatter, and its value is much lower than without the asymmetric T-slot (although still not less than 3 dB). In Step IV, another asymmetric T-slot is added. The structure design of the two asymmetric T-slots excites two orthogonal modes with equal amplitudes and a phase difference of 90°, achieving broadband characteristics and CP characteristics. This series of design adjustments, especially the introduction of the asymmetric T-slot,
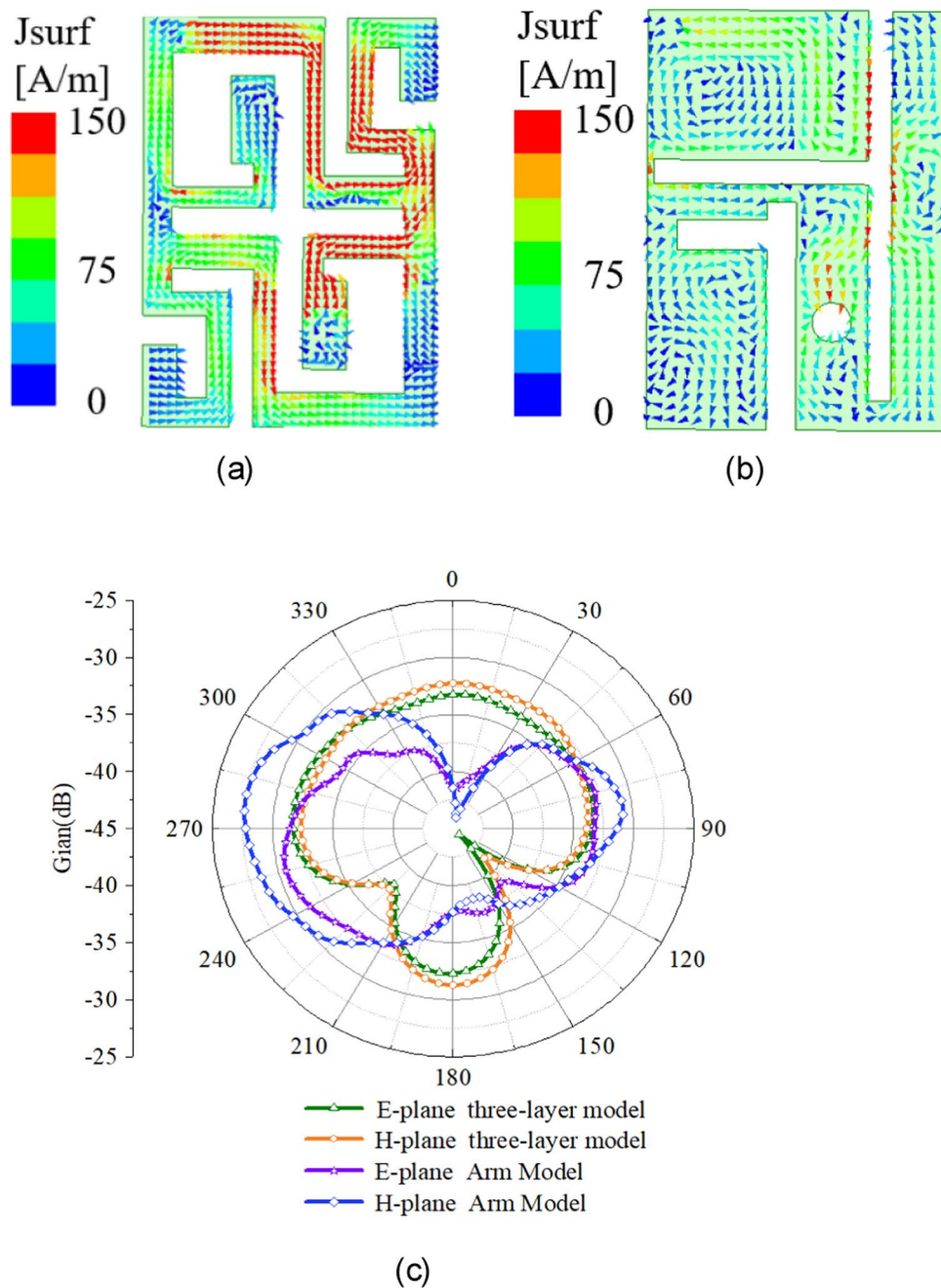
Fig. 4. (**a**) Patch current distribution. (**b**) GND current distribution. (**c**) Radiation patterns for three-layer and arm models at the 2.45 GHz frequency.

significantly improves the performance of the antenna in the desired frequency band. The $|S_{11}|$ and AR curves for each step demonstrate the evolution of the frequency and circular polarization response during the design process, highlighting the importance of the asymmetric T-slots introduced in Steps III and IV for the ultra-wideband characteristics and AR properties. Detailed information can be found in Fig. 3b–c.

Results and discussion
Antenna current distribution and radiation patterns
Figure 4a and b provides detailed information about the antenna at the 2.45 GHz frequency, the current distribution within the antenna, and the flow paths to help understand the formation and optimization of antenna performance. In the 2.45 GHz band, it is observed that the current on the patch is divided into two unidirectional flow paths. In the current distribution on the ground, it is observed that the strong currents are
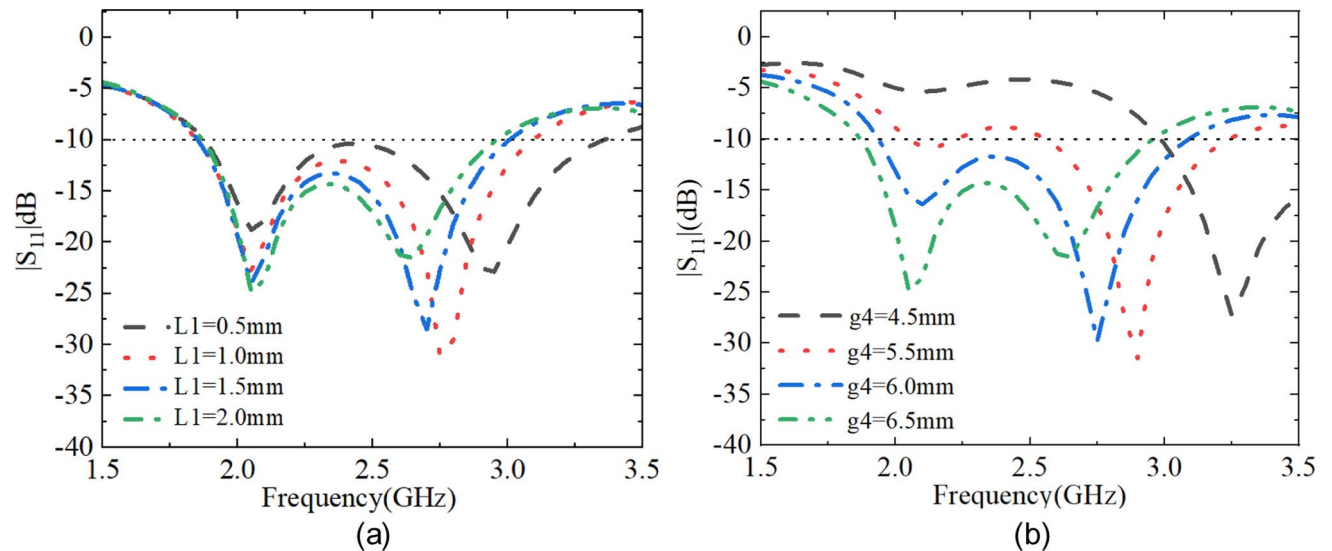
Fig. 5. (**a**) Effect of L1 change on $|S_{11}|$. (**b**) Effect of g4 change on $|S_{11}|$.

concentrated around two asymmetric T-slots, thus playing a key role in the tuning of the resonant frequency. In addition, at 2.45 GHz, the current distribution in the ground plane shows a circular path, which leads to energy loss, reducing the effective energy radiated into space by the antenna and decreasing the antenna gain. The radiation direction map under this current distribution is shown in Fig. 4c. In both the three-layer model and the arm model it has a better radiation pattern with the maximum radiation direction towards the outside of the body.

Parametric analysis

This section presents the effect of key parameters on the bandwidth and circular polarization of the designed antenna. The addition of L1 improves the impedance matching of the antenna in the ISM (2.45 GHz) operating band. the increase in g4 leads to a frequency shift towards lower frequencies and a long bandwidth of 1.85 -2.99 GHz occurs. The designed antenna achieves better performance when the parameters are optimized to L1 = 2 mm and g4 = 6.5 mm, detailed information is shown in Fig. 5a and b. Slotting not only affects the bandwidth but also the polarization; slotting introduces asymmetric current distribution and phase difference which affects the polarization of the antenna. We discuss the effect of varying the two T-slot parameters (g1, g2, g4) on the circular polarization. With increasing g1 and g4, the axial bandwidth of the antenna is shifted downwards to fully cover the operating band and the axial bandwidth increases significantly. With the increase of g2, the axial bandwidth of the antenna then covers the working band with a significant increase. The detailed information is shown in Fig. 6a–c, the circular polarization of the antenna is good when g1 = 4 mm, g2 = 4 mm and g4 = 6.5 mm.

The change of short-pin position has a great effect on the antenna $|S_{11}|$ and antenna impedance matching, which affects the resonant frequency shift and the operating bandwidth. From Fig. 6d, it can be observed that for placing the short pin in the two positions of N1 and N3, it does not satisfy the required frequency band for operation. Meanwhile, for both N3 and N4, their impedance matching performance at 2450 MHz is good. However, the overall performance of N4 is slightly better than N3, which has a wider bandwidth. More details can be obtained by observing Fig. 6d, and finally N4 is chosen as the best short pin.

Mechanism of operation of circularly polarized antenna

Figure 7b presents the 3 dB AR representing the CP characteristics. The simulated AR bandwidth of the proposed antenna in the three-layer model is 23.6% (2.36–2.94 GHz) and the measured circularly polarized bandwidth is (2.37–2.87 GHz) 20.4%. By designing the radiating surface as a structure symmetric about the center of the antenna origin[28] and introducing two asymmetric T-slots into the ground, this design excites two orthogonal modes with a 90° phase difference, resulting in circularly polarized characteristics (Fig. 8). The current distribution of the antenna provides an intuitive view to understand the circular polarization mechanism of the antenna. Figure 9 shows the current distribution of the antenna at an operating frequency of 2.45 GHZ for four phases from 0° to 270°, with the red arrows indicating the direction of the current vectors and sums at that phase angle. From the Fig. 9, it can be seen that the direction of the current combinations is all counterclockwise at this frequency, which indicates that the polarization is RHCP[29,35]. Also, the measurements in Fig. 8 show that the antenna exhibits RHCP characteristics. Good agreement is observed between the antenna's simulated and measured radiation patterns at 2.45 GHz. The difference is due to the difference between the simulated and actual test environment and the loss of the RF connecting line.
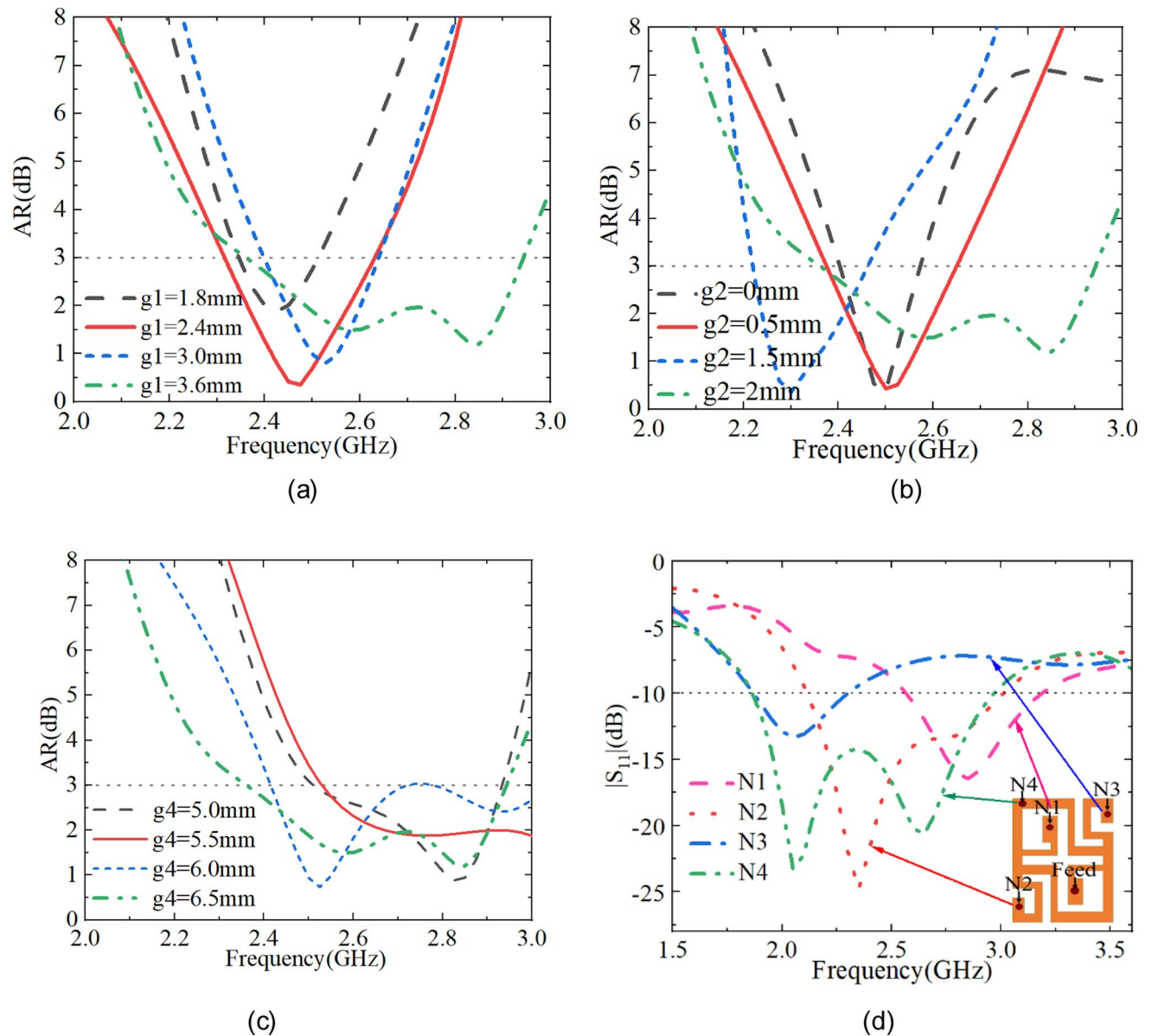
Fig. 6. (**a**) Effect of g1 change on CP. (**b**) Effect of g2 change on CP. (**c**) Effect of g4 change on CP. (**d**) Position of short pin.

SAR analysis

Furthermore, since the designed antenna operates in human tissue, safety is an important issue to be considered and is usually evaluated in terms of SAR[36]. As shown in Fig. 10, the SAR distributions in the three-layer model and the arm model are displayed in the 2.45 GHz operating band. The simulated SAR values are 652.337 W/kg and 811.425 W/Kg, respectively, at an input power of 1 W. Based on the simulated 1 g average SAR values, the input power should not exceed 2.45 mw and 1.97 mw, respectively, in order to satisfy the limitations of the IEEE standard (IEEE C95.1-2019) for 1 g average SAR.

Measurement results analysis

Figure 11 presents a physical picture of the antenna and the measurement environment. The $|S_{11}|$ in the three-layer model, right-hand arm model, and minced pork are shown in Fig. 7a. The proposed antenna resonates in the 2.45 GHz band with an impedance bandwidth of 875 MHz (1887–2762 MHz) measured in minced pork. Fabrication and soldering errors and the measured dielectric properties are not exactly the same as the simulated ones may be the reasons for the difference between the measured and simulated reflection coefficients. But the proposed antenna these broadbands adequately covers the ISM band (2400–2480 MHz). We measured the RHCP and LHCP by placing the antenna and the end of the pork in a microwave darkroom, and the results are shown in Fig. 8, where the main polarization of the antenna is the RHCP.
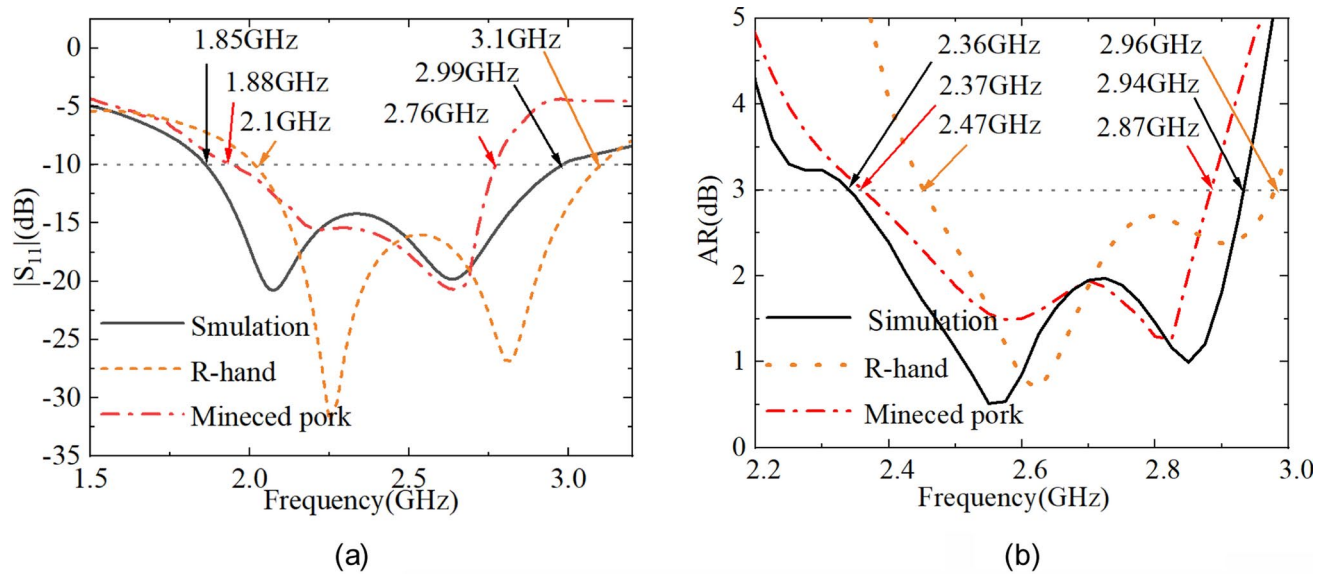
Fig. 7. Comparison of three-layer model, arm model simulation and real measurements in minced pork. (**a**) S-parameter comparison. (**b**) ARBW comparison.
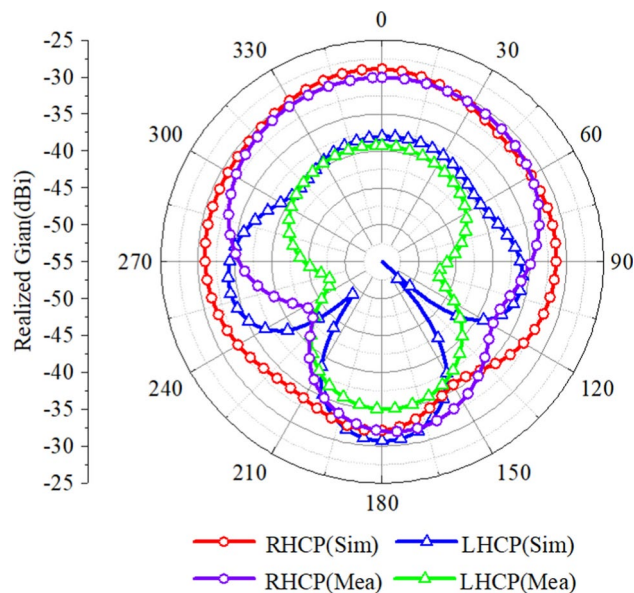

Fig. 8. Radiation patterns of RHCP and LHCP at 2.45 GHz.

Conclusions

A miniaturized ultra-wideband CP antenna for biotelemetry applications is presented. The antenna can operate in the ISM band (2.45 GHz) with circular polarization at 2.45 GHz. In addition, cross slots and multiple L-shaped slots are inserted in the radiating patch of the antenna, and two asymmetric T-shaped open slots are inserted in the ground plane, which play a key role in impedance matching, achieving circular polarization, extending AR bandwidth, and antenna size reduction. And the measurements of reflection coefficient and AR were carried out in the crushed pork. The measured results are in good agreement with the simulated results. In addition, we calculated the SAR according to the IEEE standard to ensure patient safety.
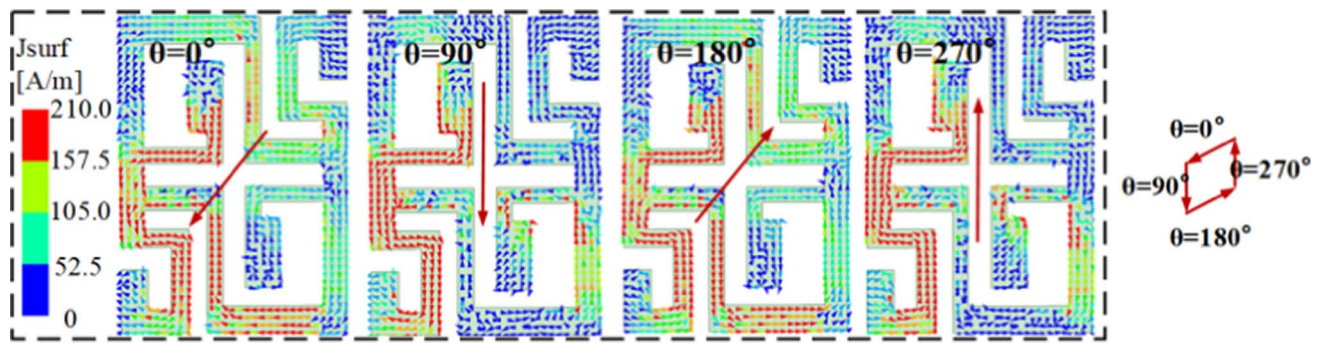
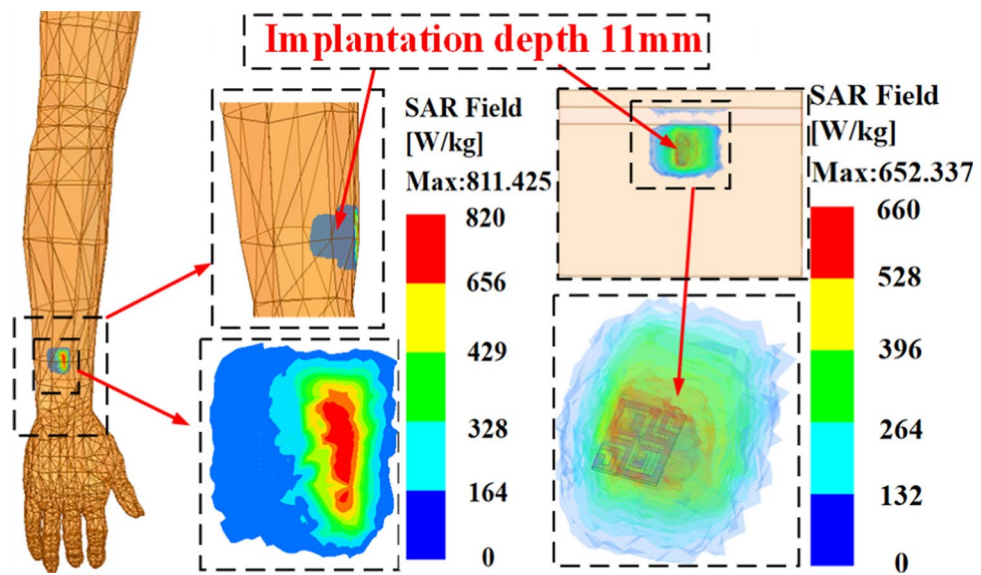**Fig. 9**. Four phase current distribution of the proposed antenna.

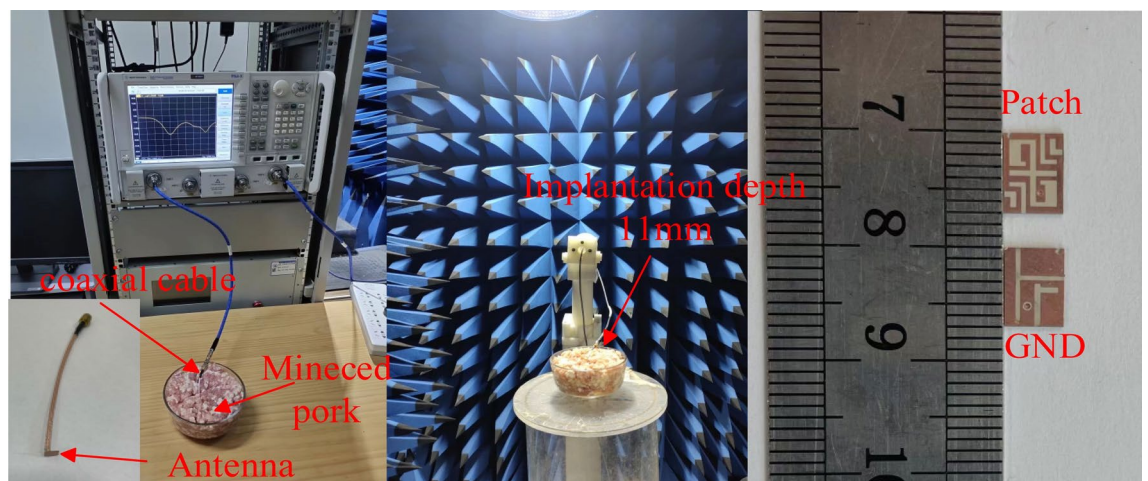**Fig. 10**. The simulated SAR distribution.

Fig. 11. Physical drawing of the antenna and the measurement environment.

Data availability

All data generated or analysed during this study are included in this article.

References

1. Liao, W., Shi, J. & Wang, J. Electromagnetic interference of wireless power transfer system on wearable electrocardiogram. *Microw. Antennas Propag.* **11**(3), 330–335 (2017).
2. Loktongbam, P., Pal, D. & Koley, C. Design of an implantable antenna for biotelemetry applications. *Microsyst. Technol.* **26**(7), 2217–2226 (2020).
3. Alrawashdeh, R. et al. A novel flexible cloud shape loop antenna for muscle implantable devices. *Elect. Eng.* **5**(1), 61–76 (2019).
4. Zainudin, N. et al. Increase of input resistance of a normal-mode helical antenna (NMHA) in human body application. *Sensors* **20**(4), 958 (2020).
5. Wang, H., Feng, Y., Hu, F. & Guo, Y. A wideband dual-polarized ring-loaded cross bowtie antenna for wireless capsule endoscopes: Design and link analysis. *IEEE Trans. Antennas Propag.* **70**(9), 7843–7852 (2022).
6. Shah, S. et al. Miniaturized four-port MIMO implantable antenna for high-data-rate wireless-capsule-endoscopy applications. *IEEE Trans. Antennas Propag.* **71**(4), 3123–3133 (2023).
7. Ramzan, M. et al. An ultra-miniaturized high efficiency implanted spiral antenna for leadless cardiac pacemakers. *IEEE Trans. Biomed. Circuits Syst.* **17**(3), 621–632 (2023).
8. Wang, M. et al. Broadband implantable antenna for wireless power transfer in cardiac pacemaker applications. *IEEE J. Electromagn. RF Microw. Med. Biol.* **5**(1), 2–8 (2021).
9. Zada, M., Shah, I. A., Basir, A. & Yoo, H. Ultra-compact implantable antenna with enhanced performance for leadless cardiac pacemaker system. *IEEE Trans. Antennas Propag.* **69**(2), 1152–1157 (2021).
10. Kiourti, A. & Nikita, K. Miniature scalp-implantable antennas for telemetry in the MICS and ISM bands: Design, safety considerations and link budget analysis. *IEEE Trans. Antennas Propag.* **60**(8), 3568–3575 (2012).
11. Salama, S., Zyoud, D. & Abuelhaija, A. Modeling of a compact dual band and flexible elliptical-shape implantable antenna in multi-layer tissue model. *Electronics* **11**(20), 3406 (2022).
12. Bahrouni, M. et al. Modeling of a compact, implantable, dual-band antenna for biomedical applications. *Electronics* **12**(6), 1475 (2023).
13. Behih, M. et al. A novel wideband and multi-band implantable antenna design for biomedical telemetry. *Appl. Comput. Electromagn. Soc. J. (ACES)* https://doi.org/10.13052/2022.ACES.J.370410 (2022).
14. Zada, M. & Yoo, H. A miniaturized triple-band implantable antenna system for bio-telemetry applications. *IEEE Trans. Antennas Propag.* **66**(12), 7378–7382 (2018).
15. Fan, Y. et al. Compact triple-broadband implantable antenna for multi-functions in telemedicine. *IET Microw. Antennas Propag.* **16**, 2–3 (2022).
16. Gupta, A. et al. A miniaturized tri-band implantable antenna for ISM/WMTS/lower UWB/Wi-Fi frequencies. *Sensors* **23**(15), 6989 (2023).
17. Shah, I. A., Zada, M. & Yoo, H. Design and analysis of a compact-sized multiband spiral-shaped implantable antenna for scalp implantable and leadless pacemaker systems. *IEEE Trans. Antennas Propag.* **67**(6), 4230–4234 (2019).
18. Abbas, N. et al. Design and measurement of a minuscule-sized implantable antenna for brain-machine interfaces. *IEEE Access* **11**, 77980 (2023).
19. Tung, L. V. & Seo, C. A miniaturized implantable antenna for wireless power transfer and communication in biomedical applications. *J. Electromagn. Eng. Sci.* **22**(4), 440 (2022).
20. Nguyen, D. & Seo, C. An ultra-miniaturized antenna using loading circuit method for medical implant applications. *IEEE Access* **9**, 111890–111898 (2021).
21. Gani, I. & Yoo, H. Multi-band antenna system for skin implant. *IEEE Microw. Wirel. Compon. Lett.* **26**(4), 294–296 (2016).
22. Shah, S. A. A. & Yoo, H. Scalp-implantable antenna systems for intracranial pressure monitoring. *IEEE Trans. Antennas Propag.* **66**(4), 2170–2173 (2018).
23. Yousaf, M. et al. Compacted conformal implantable antenna with multitasking capabilities for ingestible capsule endoscope. *IEEE Access* **8**, 157617–157627 (2020).
24. Fan, Y., Liu, X. & Xu, C. A broad dual-band implantable antenna for RF energy harvesting and data transmitting. *Micromachines* **13**(4), 563 (2022).
25. Faisal, F. et al. An ultra-miniaturized antenna with ultra-wide bandwidth for future cardiac leadless pacemaker. *IEEE Trans. Antennas Propag.* **70**(7), 5923–5928 (2022).
26. Chang, L. et al. Conformal MIMO Ultra-wideband antenna design for high-speed wireless telemetry in capsule endoscopy systems. *IEEE Trans. Antennas Propag.* **72**, 5742 (2024).
27. Samanta, G. & Mitra, D. Dual-band circular polarized flexible implantable antenna using reactive impedance substrate. *IEEE Trans. Antennas Propag.* **67**(6), 4218–4223 (2019).
28. Liu, R. P. et al. A wideband circular polarization implantable antenna for health monitor microsystem. *IEEE Trans. Antennas Propag.* **20**(5), 848 (2021).
29. Sharma, D. et al. Design and implementation of compact dual-band conformal antenna for leadless cardiac pacemaker system. *Sci. Rep.* **12**(1), 3165 (2022).
30. Kamel, Y., Mohamed, H. & ELsadek, H. Miniaturized triple-band circular polarized implantable patch antenna for bio-telemetry applications. *IEEE Antennas Wirel. Propag. Lett.* **22**(1), 74–78 (2023).
31. Lamkaddem, A., Yousfi, A. E., Abdalmalak, K. A., Posadas, V. G. & Segovia-Vargas, D. Circularly polarized miniaturized implantable antenna for leadless pacemaker devices. *IEEE Trans. Antennas Propag.* **70**(8), 6423–6432 (2022).
32. Samanta, G. & Mitra, D. Miniaturised and radiation efficient implantable antenna using reactive impedance surface for biotelemetry. *IET Microw. Antennas Propag.* **14**, 177–184 (2020).
33. Salahuddin, S. et al. Demonstration of dielectric heterogeneity of previously assumed homogeneous tissues: Examination of the heart. In *IET Conference Publications*, Vol. 2018 (2018).
34. Shaw, T., Mandal, B., Samanta, G, et al. A compact wideband biocompatible circularly polarized implantable flexible antenna for biomedical applications. In *2024 18th European Conference on Antennas and Propagation (EuCAP)* 1–4 (IEEE, 2024).
35. Hu, X. Y., Peng, H. H., Xiao, P., Gao, G. & Li, G. A novel broadband dual-frequency circularly polarized implantable antenna empowering future intelligent healthcare. *IEEE Sensors J.* **24**, 30947 (2024).
36. IEEE standard for safety levels with respect to human exposure to electric, magnetic, and electromagnetic fields, 0 Hz to 300 GHz—corrigenda 2. In *IEEE Std C95.1-2019* 1–15 (2020).

Author contributions

Methodology, Z.S. and X.Z.; software, X.Z. and Z.S.; validation, Y.W., Y.S. and X.Z.; formal analysis, Z.S. and X.Z.; writing—original draft preparation, X.Z.; writing—review and editing, Z.S.; supervision, Z.S.; project administration, Z.S.; funding acquisition, Z.S.. All authors have read and agreed to the published version of the manuscript.

Funding

Competing interests

The authors declare no competing interests.

Additional information

Correspondence and requests for materials should be addressed to Z.S.

Reprints and permissions information is available at www.nature.com/reprints.

Publisher's note Springer Nature remains neutral with regard to jurisdictional claims in published maps and institutional affiliations.